

Sparticle Spectroscopy with Neutralino Dark matter from t - b - τ Quasi-Yukawa Unification

Shahida Dar^{a,1}, Ilia Gogoladze^{b,2}, Qaisar Shafi^b and Cem Salih Ün^{b,3}

^a*Mohawk Valley Community College, 1101 Sherman Dr. Utica, NY 13501, USA*

^b*Bartol Research Institute, Department of Physics and Astronomy,
University of Delaware, Newark, DE 19716, USA*

Abstract

We consider two classes of t - b - τ quasi-Yukawa unification scenarios which can arise from realistic supersymmetric $SO(10)$ and $SU(4)_C \times SU(2)_L \times SU(2)_R$ models. We show that these scenarios can be successfully implemented in the CMSSM and NUHM1 frameworks, and yields a variety of sparticle spectra with WMAP compatible neutralino dark matter. In NUHM1 we find bino-higgsino dark matter as well as the stau coannihilation and A -funnel solutions. The CMSSM case yields the stau coannihilation and A -funnel solutions. The gluino and squark masses are found to lie in the TeV range.

¹ E-mail: shahida.dar@mvcc.edu

² E-mail: ilia@bartol.udel.edu

On leave of absence from: Andronikashvili Institute of Physics, 0177 Tbilisi, Georgia.

³ E-mail: cemsalihun@bartol.udel.edu

1 Introduction

Third family (t - b - τ) Yukawa Unification (YU, for short) at the GUT scale M_G ($\sim 3 \times 10^{16}$ GeV) is predicted by the simplest supersymmetric SO(10) GUT if the MSSM Higgs doublets are assumed to reside in the Higgs 10-plet [1]. The implications of YU for Higgs and sparticle spectroscopy have been extensively considered in the literature [2]. More recently [3], it has been argued that SO(10) GUT YU predicts relatively light ($m_{\tilde{g}} < \text{TeV}$) gluinos, which can be readily tested [4] at the Large Hadron Collider (LHC). The squarks and sleptons turn out to have masses in the multi-TeV range.

In order to reconcile radiative electroweak symmetry breaking (REWSB) with YU, the MSSM Higgs soft supersymmetry breaking (SSB) masses must be split in such way that $m_{H_d}^2/m_{H_u}^2 > 1.2$ at M_G [5]. As mentioned above, the MSSM doublets reside in the 10 dimensional representation of SO(10) GUT for YU condition to hold. In the gravity mediated supersymmetry breaking scenario [6] the required splitting in the Higgs sector can be generated by involving additional Higgs fields [7], or via D-term contributions [8]. Note that YU is sensitive not only to the value of $\tan \beta$, but also to weak scale threshold corrections [7, 9].

On the other hand, one knows that a singlet 10-plet of Higgs field does not work for the first two generations of quarks and leptons. One way to fix this problem in SO(10) is to extend the Higgs sector which couples to the SM fermions, in particular by introducing Higgs 126-plet [10]. In this case, the low energy MSSM Higgs doublets are a linear superposition of various SO(10) Higgs fields. Depending on the parameters, this may lead to deviation from exact t - b - τ YU. As pointed out in ref. [11], a relatively small deviation from t - b - τ YU (referred to here as quasi-YU) allows REWSB with universal SSB mass terms for the MSSM Higgs fields at M_G . In this paper we revisit and expand the analysis presented in [11]. We find that a modest relaxation of t - b - τ YU condition within the SO(10) GUT framework allows us to significantly lower sfermion masses which can be tested at the LHC. The quasi-YU (QYU) framework also allows one to implement the neutralino dark matter scenario consistent with the Wilkinson Microwave Anisotropy Probe (WMAP) [12] constraints. This is not possible, it appears, in SO(10) models with exact YU [3].

This paper is organized as follows. In Section 2, we present an SO(10) model which naturally yields QYU. In Section 3 we describe the scanning procedure and various SUSY constraints imposed on the parameter space of NUHM1 (non-universal Higgs model with $m_{H_u} = m_{H_d} \neq m_0$) and CMSSM (constrained minimal supersymmetric model). In Sections 4 and 5 we present our results and highlight some benchmark points of QYU condition. The correlation between direct and indirect detection of dark matter and the QYU condition is presented in Section 6. Our conclusions are summarized in Section 7.

2 The Model

One way to obtain the correct fermion masses and mixings in $SO(10)$ GUT is to utilize Higgs in the 10 and 126 dimensional representations. The Yukawa interactions in this case are given by

$$Y_{10}^{ij} 16_i \cdot 16_j \cdot H_{10} + Y_{126}^{ij} 16_i \cdot 16_j \cdot H_{\overline{126}}, \quad (1)$$

where Y_{10}^{ij} and Y_{126}^{ij} denote the Yukawa couplings. From the coupling between the $\overline{126}$ and the 10-plet Higgs, the SM doublet fields contained in $\overline{126}$ will acquire vacuum expectation values (VEVs) through mixing with the VEVs of the Higgs doublets in 10 [10]. The modification [11] of t - b - τ YU condition depends on how the doublets from the $\overline{126}$ and 10 mix and the values of Yukawa couplings in Eq. (1). One possible mixing of these doublets arises from the following interaction

$$\lambda_1 \cdot 10 \cdot \overline{126} \cdot 210 + \lambda_2 \cdot 10 \cdot 126 \cdot 210, \quad (2)$$

where λ_1 and λ_2 are dimensionless couplings. The 210-plet has an M_G scale VEV and is primarily used for breaking $SO(10)$ to its maximal subgroup $SU(4)_c \times SU(2)_L \times SU(2)_R$ [13]. However, we will exploit here the fact that there exist other M_G scale VEV directions in the 210-plet. Let us decompose the interaction in Eq. (2) in terms of the $SU(4)_c \times SU(2)_L \times SU(2)_R$ symmetry [14]

$$\begin{aligned} & \lambda_1 (1, 2, 2)_{10} (15, 2, 2)_{\overline{126}} [(15, 1, 3)_{210} + (15, 1, 1)_{210}] \\ & + \lambda_2 (1, 2, 2)_{10} (15, 2, 2)_{126} [(15, 1, 3)_{210} + (15, 1, 1)_{210}] + \dots \end{aligned} \quad (3)$$

Here we list only the relevant couplings and for simplicity, we do not consider the mixing of Higgs doublets from the 210 and 10 which does not provide any contribution to the Yukawa sector.

It was pointed out in [14] that it is possible to develop a VEV in the directions $(15, 1, 3)_{210}$ or $(15, 1, 1)_{210}$, or simultaneously in both directions. We assume that these VEVs are order of M_G . After fine tuning, one pair of Higgs doublets can be identified as the MSSM pair $(H_u + H_d)$, which, as previously stated, is an admixture of Higgs doublets from the 10 and 126. The other scalar doublets have masses of order M_G . With a non-zero VEV along the $(15, 1, 3)_{210}$ direction, the coupling $(1, 2, 2)_{10} (15, 2, 2)_{\overline{126}} (15, 1, 3)_{210}$ generates $SU(2)_R$ violating bilinear terms between the up and down type Higgs doublets, which effectively violates top-bottom YU condition at M_G . In this case, following closely the $SU(4)_C \times SU(2)_L \times SU(2)_R$ discussion in [11], one can derive the following asymptotic relations among the three Yukawa couplings:

$$y_t : y_b : y_\tau = (1 + C) : (1 - C) : (1 + 3C), \quad (\text{Case I}) \quad (4)$$

where C is taken to be real and positive. In practice, we will find that $C \sim 0.1 - 0.2$, and we refer to the QYU condition in Eq. (4) as Case I. Note that REWSB is easier to achieve for $C > 0$.

For a slightly different scenario, consider the case in which a VEV is developed only in the $(15, 1, 1)_{210}$ direction in Eq. (3). The mixing of Higgs doublets from the interaction $(1, 2, 2)_{10}(15, 2, 2)_{\overline{126}}(15, 1, 1)_{210}$ is $SU(2)_R$ invariant, and at M_G , the top-bottom YU condition still holds. In this case one finds the relation

$$y_t : y_b : y_\tau = (1 + C') : (1 + C') : (1 - 3C'), \quad (5)$$

where C' has the same definition as C , but numerically it can be different.

If the VEVs develop along both the $(15, 1, 1)_{210}$ and $(15, 1, 3)_{210}$ directions, we simply add Eqs. (4) and (5) to get [11]

$$y_t : y_b : y_\tau = (1 + C_1) : (1 - C_2) : (1 + 3C_2), \quad (\text{Case II}) \quad (6)$$

where $C_1 = C + C'$, $C_2 = C - C'$. The QYU relation given in Eq. (6) will be referred to as Case II.

3 Phenomenological constraints and scanning procedure

We employ the ISAJET 7.80 package [15] to perform random scans over the fundamental parameter space. In this package, the weak scale values of gauge and third generation Yukawa couplings are evolved to M_G via the MSSM renormalization group equations (RGEs) in the \overline{DR} regularization scheme. We do not strictly enforce the unification condition $g_3 = g_1 = g_2$ at M_G , since a few percent deviation from unification can be assigned to unknown GUT-scale threshold corrections [16]. The deviation between $g_1 = g_2$ and g_3 at M_G is no worse than 3 – 4%. For simplicity we do not include the Dirac neutrino Yukawa coupling in the RGEs, which is expected to be small.

The various boundary conditions are imposed at M_G and all the SSB parameters, along with the gauge and Yukawa couplings, are evolved back to the weak scale M_Z . In the evaluation of Yukawa couplings the SUSY threshold corrections [17] are taken into account at the common scale $M_{\text{SUSY}} = \sqrt{m_{\tilde{t}_L} m_{\tilde{t}_R}}$. The entire parameter set is iteratively run between M_Z and M_{GUT} using the full 2-loop RGEs until a stable solution is obtained. To better account for leading-log corrections, one-loop step-beta functions are adopted for gauge and Yukawa couplings, and the SSB parameters m_i are extracted from RGEs at multiple scales $m_i = m_i(m_i)$. The RGE-improved 1-loop effective potential is minimized at an optimized scale M_{SUSY} , which effectively

accounts for the leading 2-loop corrections. Full 1-loop radiative corrections are incorporated for all sparticle masses.

The requirement of REWSB puts an important theoretical constraint on the parameter space. Another important constraint comes from limits on the cosmological abundance of stable charged particles [18]. This excludes regions in the parameter space where charged SUSY particles, such as $\tilde{\tau}_1$ or \tilde{t}_1 , become the lightest supersymmetric particle (LSP). We accept only those solutions for which one of the neutralinos is the LSP and saturates the WMAP dark matter relic abundance bound.

We have performed random scans for the following parameter range:

$$\begin{aligned}
0 &\leq m_0 \leq 20 \text{ TeV} \\
0 &\leq m_{H_u} = m_{H_d} \leq 20 \text{ TeV} \\
0 &\leq M_{1/2} \leq 3 \text{ TeV} \\
45 &\leq \tan \beta \leq 60 \\
-3 &\leq A_0/m_0 \leq 3
\end{aligned} \tag{7}$$

with $\mu > 0$ and $m_t = 173.1 \text{ GeV}$ [19] with $m_0 \neq m_{H_u, H_d}$, this is usually referred to as NUHM1 [20]. This choice of parameter space was informed by our previous experience studying exact t - b - τ YU [7, 9]. In section 5, we will consider the well-known case of CMSSM with $m_0 = m_{H_u, H_d}$. In contrast to NUHM1, we are unable to identify bino-Higgsino dark matter in the CMSSM framework with QYU.

Our results are not too sensitive to one or two sigma variation in the value of m_t [7]. We use $m_b(m_Z) = 2.83 \text{ GeV}$ which is hard-coded into ISAJET.

In scanning the parameter space, we employ the Metropolis-Hastings algorithm as described in [21]. All of the collected data points satisfy the requirement of REWSB, with the neutralino in each case being the LSP. Furthermore, all of these points satisfy the constraint $\Omega_{\text{CDM}} h^2 \leq 10$. This is done so as to collect more points with a WMAP compatible value of cold dark matter (CDM) relic abundance. For the Metropolis-Hastings algorithm, we only use the value of $\Omega_{\text{CDM}} h^2$ to bias our search. Our purpose in using the Metropolis-Hastings algorithm is to be able to search around regions of acceptable $\Omega_{\text{CDM}} h^2$ more fully. After collecting the data, we impose the mass bounds on all the particles [18] and use the IsaTools package [22] to implement the following phenomenological constraints: We apply the following experimental constraints successively on the data that we acquire from ISAJET:

$$\begin{aligned}
m_h \text{ (lightest Higgs mass)} &\geq 114.4 \text{ GeV} & [23] \\
BR(B_s \rightarrow \mu^+ \mu^-) &< 5.8 \times 10^{-8} & [24] \\
2.85 \times 10^{-4} \leq BR(b \rightarrow s \gamma) &\leq 4.24 \times 10^{-4} \text{ (} 2\sigma \text{)} & [25] \\
0.15 \leq \frac{BR(B_u \rightarrow \tau \nu_\tau)_{\text{MSSM}}}{BR(B_u \rightarrow \tau \nu_\tau)_{\text{SM}}} &\leq 2.41 \text{ (} 3\sigma \text{)} & [25] \\
\Omega_{\text{CDM}} h^2 &= 0.111^{+0.028}_{-0.037} \text{ (} 5\sigma \text{)} & [12]
\end{aligned}$$

For $BR(B_s \rightarrow s\gamma)$ we use 2σ significance because it is relatively well measured by several experiments. Moreover, it is commonly used by several authors, and so we have considered the constraint on $BR(B_s \rightarrow s\gamma)$ to the same significance order as some other studies.

We use 3σ significance for $\frac{BR(B_u \rightarrow \tau\nu_\tau)_{\text{MSSM}}}{BR(B_u \rightarrow \tau\nu_\tau)_{\text{SM}}}$ because this ratio suffers from large uncertainties in the determination of $|V_{ub}|$. It is also commonly used in the literature.

We use 5σ significance for $\Omega_{\text{CDM}}h^2$ constraints because the co-annihilation process for calculating the relic abundance is an exponential function of the difference in masses between the LSP and the NLSP. A slight change in this mass difference can produce large uncertainties. We therefore think that 5σ is an appropriate and conservative range to take for $\Omega_{\text{CDM}}h^2$.

4 Quasi-Yukawa Unification and Sparticle Spectroscopy in NUHM1

4.1 Case I

In Fig. 1 we present our results in the $M_{1/2}-m_0$, $M_{1/2}-\tan\beta$, A_0/m_0-m_0 , $m_0-\tan\beta$ planes. The gray points are consistent with REWSB and χ_1^0 LSP, and the light blue points satisfy the QYU constraint given in Eq. (4). The green points are a subset of blue points and satisfy particle mass bounds and constraints from $BR(B_s \rightarrow \mu^+\mu^-)$, $BR(B_u \rightarrow \tau\nu_\tau)$ and $BR(b \rightarrow s\gamma)$. In addition, we require that these points do no worse than the SM in terms of the $(g-2)_\mu$ prediction. The yellow points belong to the subset of green points that satisfy all constraints including the WMAP observed dark matter density. From the $M_{1/2}-\tan\beta$ and $m_0-\tan\beta$ planes we see that realistic solutions arise for $m_0 \gtrsim 500$ GeV and $M_{1/2} \gtrsim 600$ GeV. The A_0/m_0-m_0 plane shows that in contrast to t - b - τ YU, QYU does not have a preferred value for A_0/m_0 [3], and viable solutions can be obtained for $|A_0/m_0| \gtrsim 2$.

In Fig. 2, we present some results pertaining to the parameter C with the same color coding as Fig. 1. We observe that C as small as 0.12 is compatible with all experimental constraints (yellow points). The lower bound on C is dictated mostly by the REWSB condition. As mentioned above, we have a universal Higgs SSB bilinear term ($m_{H_u} = m_{H_d}$) at M_G . In this case, for REWSB the Yukawa coupling y_t has to be larger than the Yukawa coupling y_b between M_G and M_Z . In the data that we have collected satisfying the QYU condition in the NUHM1 parameter space, we find that $y_t - y_b \gtrsim 0.1$. This, according to Eq. (4), is equivalent to $C \gtrsim 0.12$.

It was pointed out in ref. [7] that it is hard to have $y_t > 0.6$. To see this let us consider the SUSY threshold corrections to the top quark mass. The leading

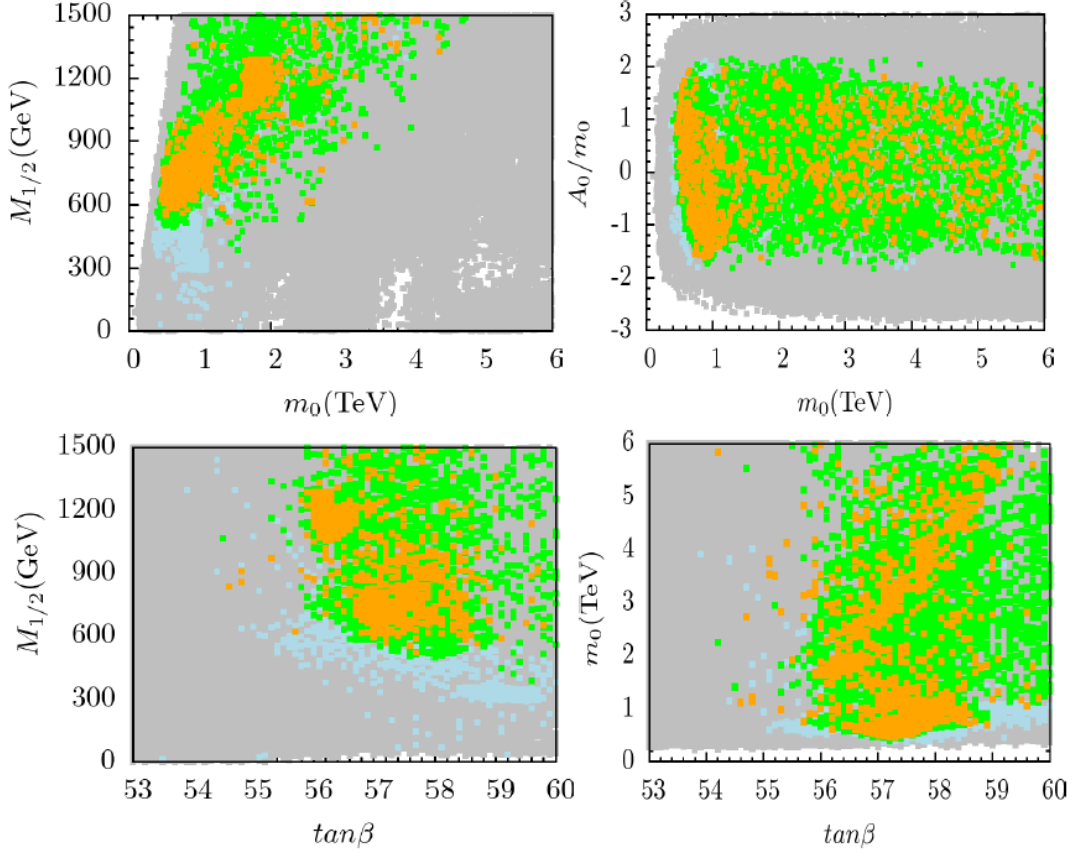


Figure 1: Plots in the $M_{1/2} - m_0$, $M_{1/2} - \tan\beta$, $A_0/m_0 - m_0$, $m_0 - \tan\beta$ planes for Case I. Gray points are consistent with REWSB and χ_1^0 LSP. Light blue points satisfy the QYU constraint given in Eq. (4). The green points satisfy particle mass bounds and constraints from $BR(B_s \rightarrow \mu^+\mu^-)$, $BR(B_u \rightarrow \tau\nu_\tau)$ and $BR(b \rightarrow s\gamma)$. In addition, we require that these points do no worse than the SM in terms of the $(g-2)_\mu$ prediction. Yellow points belong to the subset of green points that satisfies all constraints including dark matter ones from WMAP.

correction is given by [17]

$$\delta y_t^{\text{finite}} \approx \frac{g_3^2}{12\pi^2} \frac{\mu m_{\tilde{g}} \tan\beta}{m_t^2}. \quad (8)$$

In our sign convention (evolving the couplings from M_G to M_Z), a negative contribution to δy_t is preferred. Naively, a larger negative contribution allows for a larger $y_t(M_G)$. However, in the case of same sign gauginos with $\mu > 0$, we get a positive

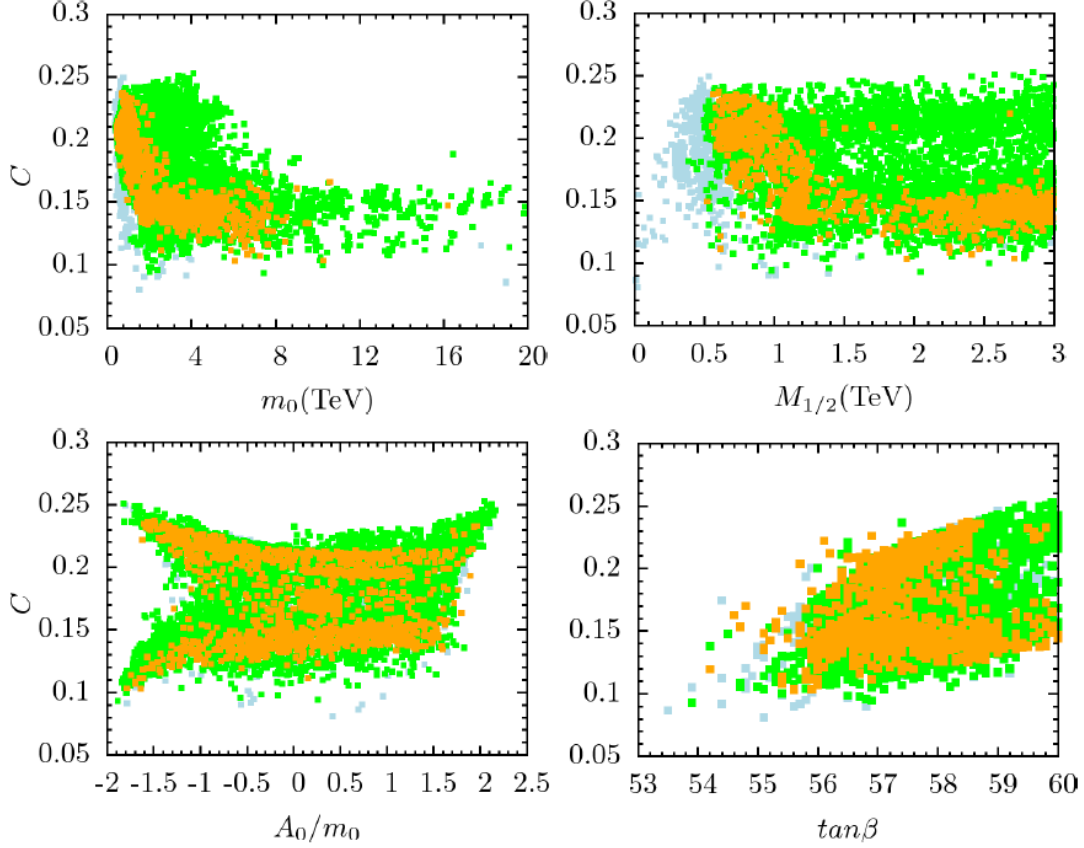


Figure 2: Plots in the $C - m_0$, $C - M_{1/2}$, $C - A_0/m_0$, $C - \tan \beta$ planes for Case I. Color coding is the same as in Fig. 1.

contribution to δy_t , thus a large m_0 value is required in order to minimize the contribution coming from Eq. (8). The significance of looking at the sign of the correction to δy_t in this case is the realization that it may not be possible to achieve $y_t > 0.6$. On the other hand, despite the possibility for large thresholds for the large bottom quark, one may not have arbitrarily small values for y_b at M_G . From the data we find that $y_b(M_G)$ cannot be much smaller than 0.35 or so. If we use the maximal value for y_t and the minimal value for y_b in the expression $C = (y_t - y_b)/(y_t + y_b)$ (which can be derived from Eq. (4)), we see that $C \gtrsim 0.25$.

In Fig. 3, we show the relic density channels consistent with QYU condition (Eq. (4)) in the $m_{\tilde{\chi}_1^\pm} - m_{\tilde{\chi}_1^0}$, $m_{\tilde{\tau}} - m_{\tilde{\chi}_1^0}$ and $m_A - m_{\tilde{\chi}_1^0}$ planes. The dark green points in this figure satisfy the requirements of REWSB, $\tilde{\chi}_1^0$ LSP, the particle mass bounds and constraints from $BR(B_s \rightarrow \mu^+ \mu^-)$, $BR(B_u \rightarrow \tau \nu_\tau)$ and $BR(b \rightarrow s \gamma)$.

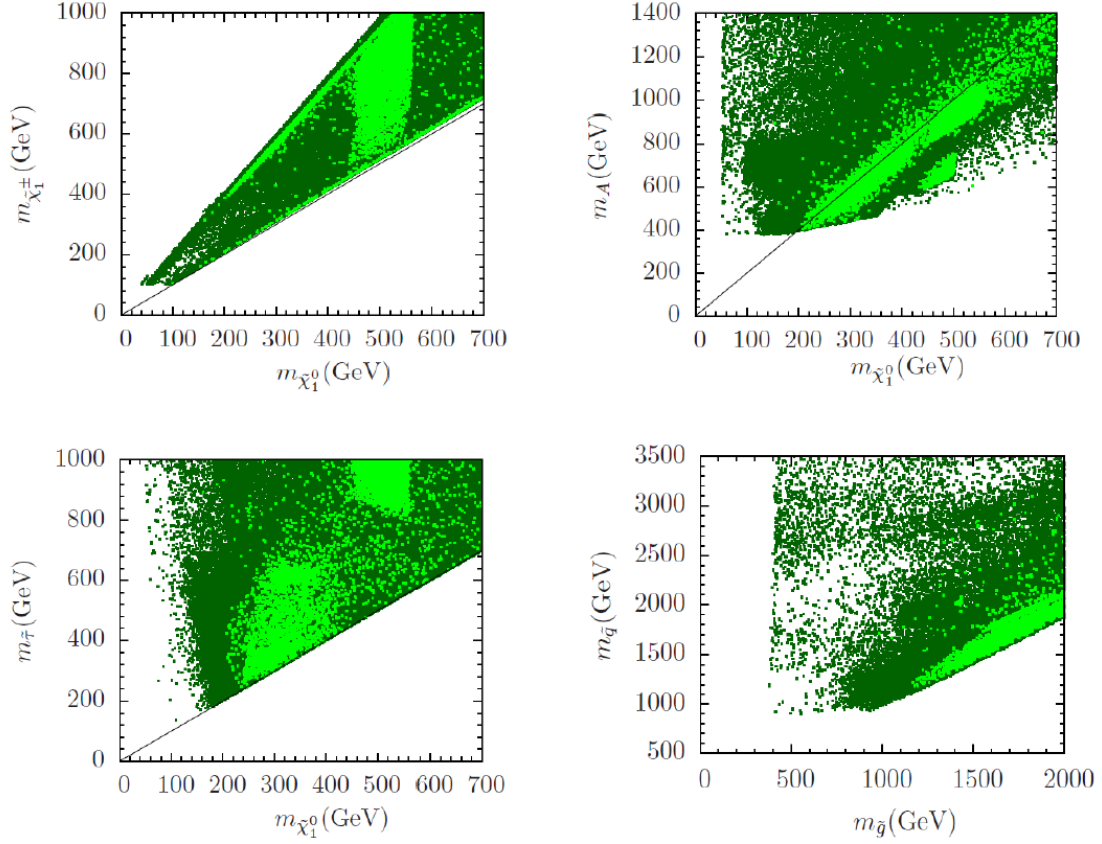


Figure 3: Plots in the $m_{\tilde{\chi}_1^\pm} - m_{\tilde{\chi}_1^0}$, $m_A - m_{\tilde{\chi}_1^0}$, $m_{\tilde{\tau}} - m_{\tilde{\chi}_1^0}$ and $m_{\tilde{q}} - m_{\tilde{g}}$ planes for Case I. The dark green points in this figure satisfy the requirements of REWSB, $\tilde{\chi}_1^0$ LSP, the particle mass bounds and constraints from $BR(B_s \rightarrow \mu^+\mu^-)$, $BR(B_u \rightarrow \tau\nu_\tau)$ and $BR(b \rightarrow s\gamma)$ in NUHM1. In addition, we require that these points do no worse than the SM in terms of the $(g-2)_\mu$ prediction. The light green points are consistent with QYU condition and constraints mentioned above. We show in the $m_{\tilde{\chi}_1^\pm} - m_{\tilde{\chi}_1^0}$, and $m_{\tilde{\tau}} - m_{\tilde{\chi}_1^0}$ planes the unit slope lines that indicate the respective coannihilation channels. In the $m_A - m_{\tilde{\chi}_1^0}$ plane we show the line $m_A = 2m_{\tilde{\chi}_1^0}$ that signifies the A -funnel solution.

In addition, we require that these points do no worse than the SM in terms of the $(g-2)_\mu$ prediction. The light green points are consistent with QYU condition and the constraints mentioned above. We can see in Fig. 3 that a variety of coannihilation and annihilation scenarios are compatible with QYU and neutralino dark matter. Included in the $m_A - m_{\tilde{\chi}_1^0}$ plane is the line $m_A = 2m_{\tilde{\chi}_1^0}$ which shows that the A -funnel solution is compatible with the QYU condition. In the $m_{\tilde{\chi}_1^\pm} - m_{\tilde{\chi}_1^0}$, $m_{\tilde{\tau}} - m_{\tilde{\chi}_1^0}$

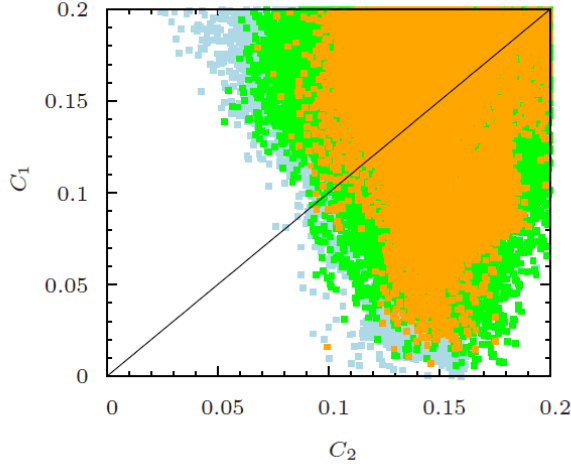


Figure 4: Plots in the $C_1 - C_2$ planes for Case II. Color coding is the same as in Fig. 1.

planes in Fig. 3, we draw the unit slope line which indicates the presence of stau coannihilation and bino-Higgsino mixed dark matter scenarios. We can see how the parameter space is reduced once QYU condition is applied. In Fig. 3 we also present results in the $m_{\tilde{g}} - m_{\tilde{q}}$ plane. It shows that QYU condition predicts relatively heavy gluinos and the first two family squarks ($m_{\tilde{g},\tilde{q}} > 1$ TeV).

4.2 Case II

As we saw in Fig. 1, the QYU condition presented in Eq. (4) strongly squeezes the allowed fundamental parameter space (light blue points) compared to the parameter space for NUHM1 (gray points) in the absence of this condition. On the other hand, the relation presented in Eq. (6) is quite common in SO(10) model building. We find that with completely arbitrary values for the parameters C_1 and C_2 in Eq. (6), the allowed parameter space is very similar to what we have for NUHM1. However, arbitrary values for C_1 and C_2 contradict our strategy, which is to have as small a deviation as possible from exact t - b - τ YU. Thus, we impose $C_1 < 0.2$ and $C_2 < 0.2$ in case II.

In Fig. 4 we present our results in the $C_1 - C_2$ plane. The color coding is the same as in Fig. 1. The parameter C_1 can be as small as 0.01, while it is hard to find C_2 values less than 0.1.

In Fig. 5 we present our results in the $M_{1/2} - m_0$, $M_{1/2} - \tan\beta$, $A_0/m_0 - m_0$, $m_0 - \tan\beta$ planes for $C_1 < 0.2$ and $C_2 < 0.2$. The color coding is the same as in Fig. 1. We can see that the allowed parameter space is increased compared to Case

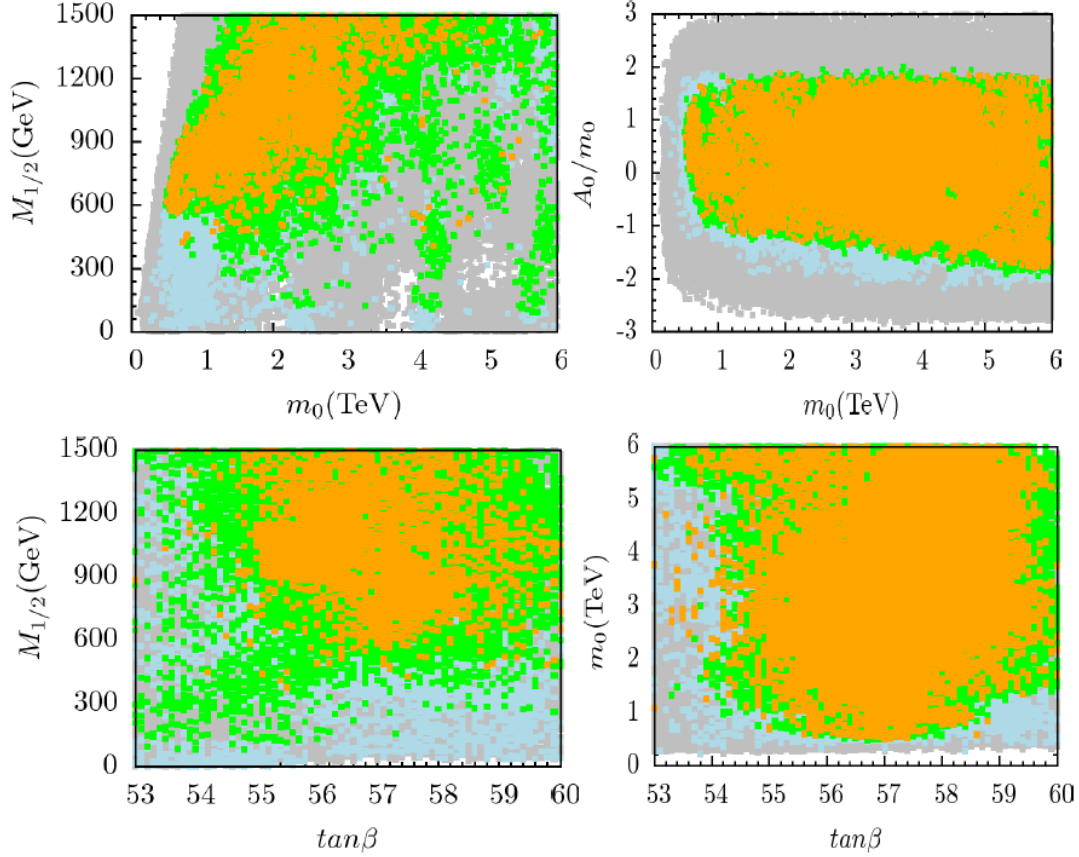


Figure 5: Plots in the $M_{1/2} - m_0$, $M_{1/2} - \tan\beta$, $A_0/m_0 - m_0$, $m_0 - \tan\beta$ planes for Case II. Color coding is the same as in Fig. 1.

I in Fig. 1. The lower bound for $M_{1/2}$ satisfying all constraints except the WMAP dark matter relic density bound is almost twice as small compared to Case I.

The differences in the allowed parameter space between Case I and Case II become more visible when we compare Fig. 3 and 6. The LSP neutralino in Case II can be as light as 50 GeV or so, while for Case I the corresponding lower bound is $m_{\tilde{\chi}_1^0} \approx 200$ GeV. The $m_{\tilde{\chi}_1^\pm} - m_{\tilde{\chi}_1^0}$ plane shows that there are plenty of bino-Higgsino dark matter solutions.

In Table 1 we present some benchmark points for the SO(10) QYU scenario implemented in NUHM1. All of these points are consistent with neutralino dark matter and the constraints mentioned in Section 3. For Point 1 bino-Higgsino mixing plays a major role in giving the correct dark matter relic density. Point 2 corresponds to the A -funnel solution, while point 3 represents the stau coannihilation channel. Point 4

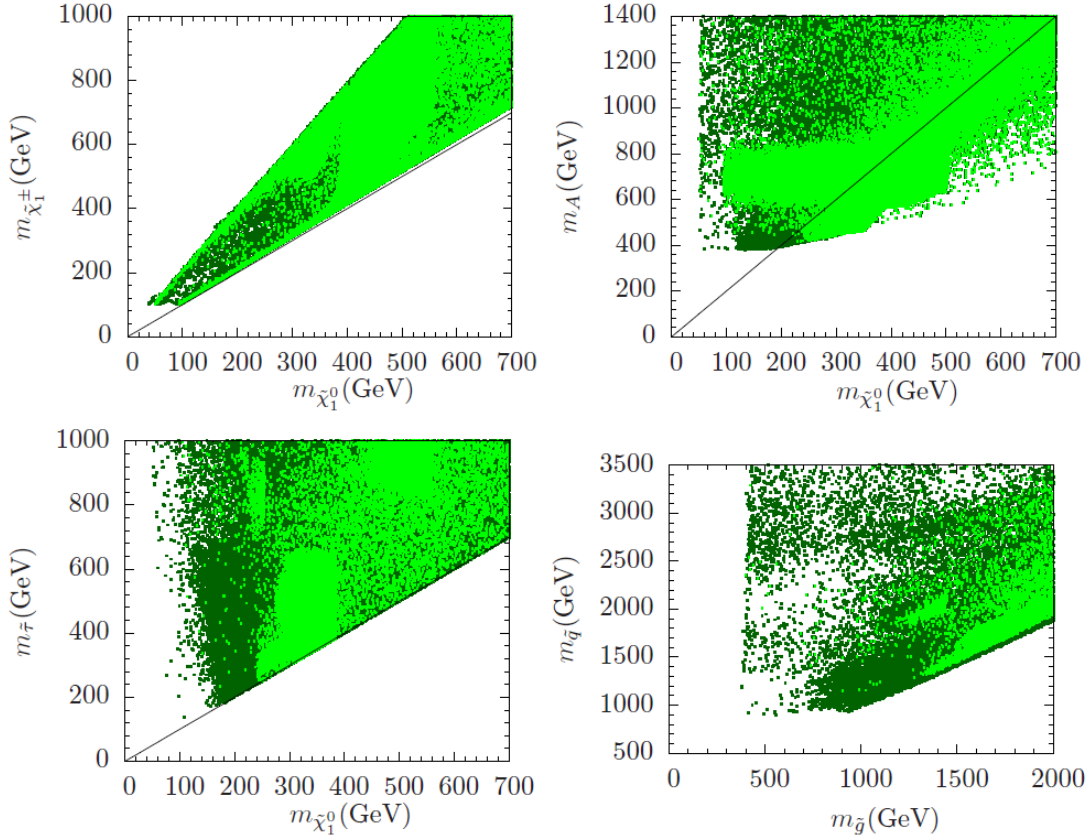


Figure 6: Plots in the $m_{\tilde{\chi}_1^\pm} - m_{\tilde{\chi}_1^0}$, $m_A - m_{\tilde{\chi}_1^0}$, $m_{\tilde{\tau}} - m_{\tilde{\chi}_1^0}$ and $m_{\tilde{q}} - m_{\tilde{g}}$ planes for Case II. Color coding is the same as in Fig. 3.

represents Case II where $C_1 + C_2$ is taken to be minimal, which is equivalent to have minimal deviation between y_t and y_b at M_G . As expected [28], both the spin independent and spin dependent cross sections of the neutralinos on protons are larger for Point 1.

5 Quasi-Yukawa Unification and Sparticle Spectroscopy: CMSSM

The CMSSM is one of the most popular frameworks for studying the low scale sparticle spectroscopy, and we therefore, discuss it here in light of QYU. Following the NUHM1 case, we perform random scans for the parameter range presented in Eq. (7) with the additional constraint $m_0 = m_{H_u} = m_{H_d}$.

	Point 1	Point 2	Point 3	Point 4
m_0	3535	838.2	781.9	1123
$M_{1/2}$	1585	674.30	970.40	741.5
$\tan \beta$	55.1	58.1	58.2	57.5
A_0/m_0	-0.42	1.09	0.82	0.72
$m_{Hu} = m_{Hd}$	4149	254	727	1375
m_t	173.1	173.1	173.1	173.1
$\text{sgn } \mu$	+	+	+	+
m_h	118.26	113.45	115.44	113.94
m_H	1714.9	546.76	703.34	476.79
m_A	1703.7	543.15	698.72	473.65
m_{H^\pm}	1717.4	553.90	709.12	485.54
$m_{\tilde{\chi}_{1,2}^0}$	623.45, 640.99	284.27, 542.35	414.82, 780.93	310.49, 471.73
$m_{\tilde{\chi}_{3,4}^0}$	715.69, 1336.9	960.6, 966.75	1035.9, 1046.8	492.56, 628.32
$m_{\tilde{\chi}_{1,2}^\pm}$	651.21, 1315.8	543.08, 967.24	781.53, 1047.2	475.95, 620.41
$m_{\tilde{g}}$	3522.8	1549.9	2147.9	1699.3
$m_{\tilde{u}_{L,R}}$	4635.6, 4564.6	1613.5, 1571.9	2086.6, 2016.9	1875.3, 1833.5
$m_{\tilde{t}_{1,2}}$	3068.4, 3512.5	1292, 1447.6	1640.2, 1848.5	1361, 1534.1
$m_{\tilde{d}_{L,R}}$	4636.3, 4556.3	1615.6, 1567.1	2088.2, 2009.6	1877.1, 1829
$m_{\tilde{b}_{1,2}}$	3488.9, 3605.3	1377.5, 1458.6	1759.6, 1843.1	1483.3, 1531.1
$m_{\tilde{\nu}_1}$	3678.2	946.72	1008.6	1221.9
$m_{\tilde{\nu}_3}$	2821.6	799.49	830.01	891.31
$m_{\tilde{e}_{L,R}}$	3678.8, 3579.3	950.80, 874.37	1013.1, 860.08	1224.9, 1155.3
$m_{\tilde{\tau}_{1,2}}$	2198, 2820.9	533.66, 819.86	427.96, 847.75	530.84, 897.20
$\sigma_{SI}(\text{pb})$	0.17915×10^{-7}	0.14364×10^{-8}	0.73529×10^{-9}	0.27819×10^{-7}
$\sigma_{SD}(\text{pb})$	0.11476×10^{-4}	0.89996×10^{-7}	0.88293×10^{-7}	0.48096×10^{-5}
$\Omega_{CDM} h^2$	0.086	0.074	0.118	0.108
C	0.15	0.21	0.19	$C_1=0.03, C_2=0.14$

Table 1: Sparticle and Higgs masses (in GeV). All of these benchmark points satisfy the various constraints mentioned in Section 3 and are compatible with QYU in the NUHM1 framework. LSP in Point 1 is a bino-Higgsino admixture, while Point 2 corresponds to the A -funnel solution. Point 3 represents the stau coannihilation channel. Point 4 represents Case II with minimal value of $C_1 + C_2$.

In Fig. 7 we present our results in the $M_{1/2} - m_0$, $M_{1/2} - \tan \beta$, $A_0/m_0 - m_0$ and $m_0 - \tan \beta$ planes for the CMSSM case. The color coding is the same as in Fig. 1. We can see that the allowed parameter space is restricted compared to what we have for Case I in Fig. 1. In good approximation we can say that QYU predicts $\tan \beta \approx 57$

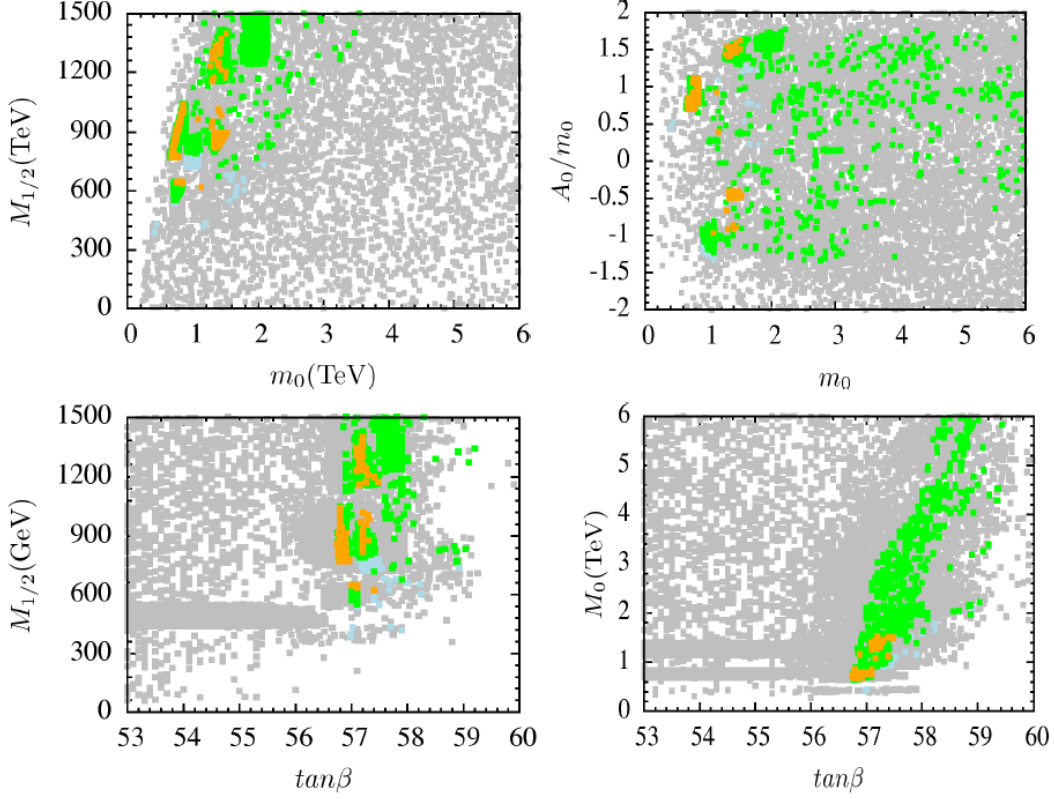


Figure 7: Plots in the $M_{1/2} - m_0$, $M_{1/2} - \tan\beta$, $A_0/m_0 - m_0$, $m_0 - \tan\beta$ planes for the CMSSM. Color coding is the same as in Fig. 1.

which is compatible with all collider and WMAP bounds. Also QYU prefers smaller value for $m_0 < 2$ TeV while precise t - b - τ YU with universal gaugino masses prefers $m_0 \gtrsim 6$ TeV [3]. There is no preference for A_0/m_0 value in contrast to the precise t - b - τ YU.

In Fig. 8, we present our results in the $C - m_0$, $C - M_{1/2}$, $C - A_0/m_0$, $C - \tan\beta$ planes. Color coding is the same as Fig. 1. A comparison with Fig. 2 shows that the allowed value of C is significantly constrained to ~ 0.2 . In contrast to NUHM1, we are unable to find bino-Higgsino dark matter in the CMSSM framework with QYU. But as we can see in Fig. 9, there are plenty of stau coannihilation and A -funnel solution.

In Table 2 we present some benchmark points for QYU in the CMSSM framework. All of these points are consistent with neutralino dark matter and the constraints mentioned in Section 3. Point 2 corresponds to the stau coannihilation channel and Point 3 represents A -funnel solution.

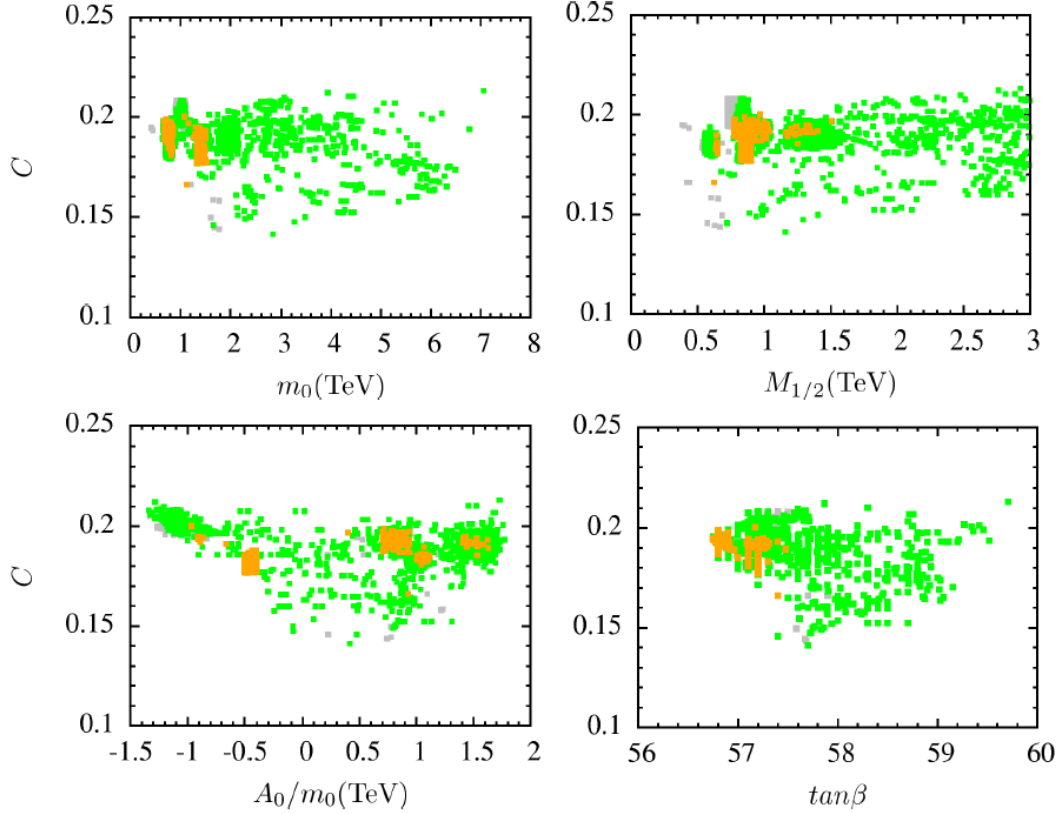


Figure 8: Plots in the $C - m_0$, $C - M_{1/2}$, $C - A_0/m_0$, $C - \tan\beta$ planes for the CMSSM. Color coding is the same as in Fig. 1.

6 Quasi-Yukawa Unification and Dark Matter Detection

In light of the recent results by the CDMS-II [26] and Xenon100 [27] experiments, it is important to see if QYU, within the NUHM1 and CMSSM frameworks presented in this paper, is testable from the perspective of direct and indirect detection experiments. The question of interest is whether $\mu \sim M_1$ is consistent with QYU, as this is the requirement to get a bino-Higgsino admixture for the lightest neutralino which, in turn, enhances both the spin dependent and spin independent neutralino-nucleon scattering cross sections [28]. In Fig.10 for Case I and Fig.11 for Case 2, we show the spin independent and spin dependent cross sections as a function of the LSP neutralino mass. In the $\sigma_{\text{SI}} - m_{\tilde{\chi}_1^0}$ plane, the current and future bounds are represented by black (solid and dashed) lines for the CDMS experiment [29] and by red (solid and dashed) lines for the Xenon experiment. The color coding is the same as

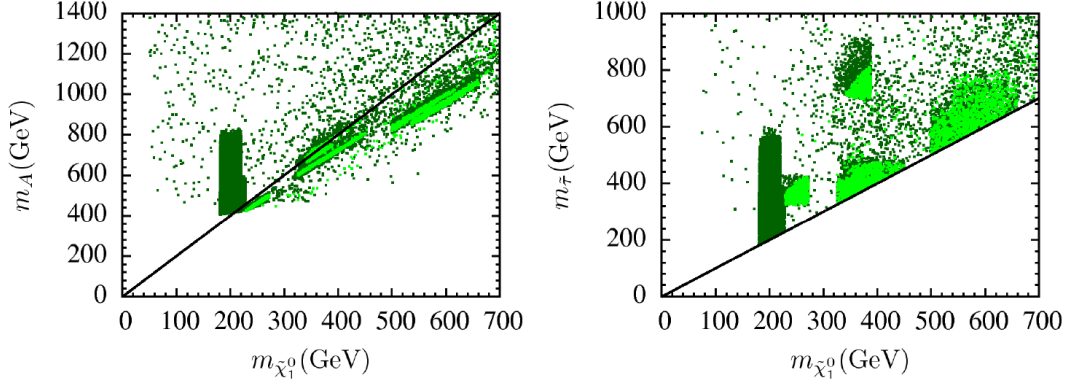


Figure 9: Plots in the $m_A - m_{\tilde{\chi}_1^0}$ and $m_{\tilde{\tau}} - m_{\tilde{\chi}_1^0}$ planes for the CMSSM case. Color coding is the same as in Fig. 3.

in Fig. 1. For Case II a small region of the parameter space consistent with QYU and the experimental constraints discussed in Section 3 is at the exclusion limits set by the recent CDMS and XENON experiments. Thus, the ongoing and planned direct detection experiments will play a vital role in testing QYU. Note that the above remarks only apply to NUHM1 which contains bino-Higgsino dark matter solutions.

For the spin dependent cross section, we show in Figs. 10 and 11 the current bounds from the Super-K (black line) [30] and IceCube (dotted red line) [31] experiments and the projected future reach of IceCube DeepCore (red solid line). The current Super-K and IceCube bounds are not stringent enough to rule out the parameter space characteristic for NUHM1 with QYU. However, from Figs. 10 and 11 we observe that the IceCube DeepCore experiment should be able to constrain some region of the parameter space, especially for Case II.

In Figure 12, we show the spin independent cross section as a function of $BR(B_s \rightarrow \mu^+ \mu^-)$ for case I (left panel) and Case II (right panel) in the NUHM1 parameter space. Gray points are consistent with REWSB and neutralino LSP. Red points are a subset of gray points which are excluded by Xenon100 and CDMS-II experiments. Blue points belong to a subset of gray points and they can be tested by Xenon100 experiment. Red and blue points are both consistent with QYU and the experimental constraints discussed in Section 3. The blue points correspond to the orange points which are located between the dashed and solid red lines in Figure 10 and Figure 11 in $\sigma_{SI} - m_{\tilde{\chi}_1^0}$ panel. According to LHCb results, the lower bound on the rare decay $BR(B_s \rightarrow \mu^+ \mu^-)$ approaches its SM limit, which means that supersymmetric contribution has to get smaller. This is the reason why we have a big interval for the neutralino nucleon cross section when $2.3 \times 10^{-9} < BR(B_s \rightarrow \mu^+ \mu^-) < 1.2 \times 10^{-8}$.

	Point 1	Point 2
m_0	692.6	1395
$M_{1/2}$	804.3	855.1
$\tan \beta$	56.8	57.2
A_0/m_0	0.76	-0.42
m_t	173.1	173.3
$\text{sgn } \mu$	+	+
m_h	117.5	119
m_H	635.1	715.3
m_A	630.9	710.6
m_{H^\pm}	641.5	721.1
$m_{\tilde{\chi}_{1,2}^0}$	340.5, 641.5	368.2, 698.3
$m_{\tilde{\chi}_{3,4}^0}$	866.1, 878.9	1025.3, 1034
$m_{\tilde{\chi}_{1,2}^\pm}$	642, 879.1	699, 1034.2
$m_{\tilde{g}}$	1806.4	1952.1
$m_{\tilde{u}_{L,R}}$	1768.8, 1712.6	2210, 2162.9
$m_{\tilde{t}_{1,2}}$	1362.8, 1561.8	1544.4, 1800.9
$m_{\tilde{d}_{L,R}}$	1770.8, 1706.9	2211.5, 2157.5
$m_{\tilde{b}_{1,2}}$	1486, 1560.1	1746.6, 1827.2
$m_{\tilde{\nu}_1}$	870.8	1501.7
$m_{\tilde{\nu}_3}$	742.7	1239.3
$m_{\tilde{e}_{L,R}}$	875.6, 754	1504.2, 1429.4
$m_{\tilde{\tau}_{1,2}}$	358.5, 760	755.1, 1245.3
$\sigma_{SI}(\text{pb})$	0.13×10^{-8}	0.56×10^{-9}
$\sigma_{SD}(\text{pb})$	0.27×10^{-6}	0.13×10^{-6}
$\Omega_{CDM} h^2$	0.11	0.10
C	0.19	0.18

Table 2: Sparticle and Higgs masses (in GeV). These benchmark points satisfy the various constraints mentioned in Section 3 and are compatible with QYU in the CMSSM framework. Point 1 corresponds to the stau coannihilation channel, while Point 2 represents the A -funnel solution.

7 Conclusion

We have explored quasi or approximate third family t - b - τ YU predicted in a class of realistic $SO(10)$ and $SU(4)_c \times SU(2)_L \times SU(2)_R$ models. We find that QYU when implemented in a NUHM1 setup is compatible with the bino-Higgsino dark matter as well as the stau coannihilation and the A -funnel solutions. We could not identify a bino-Higgsino dark matter solution in the CMSSM case in the parameter range that

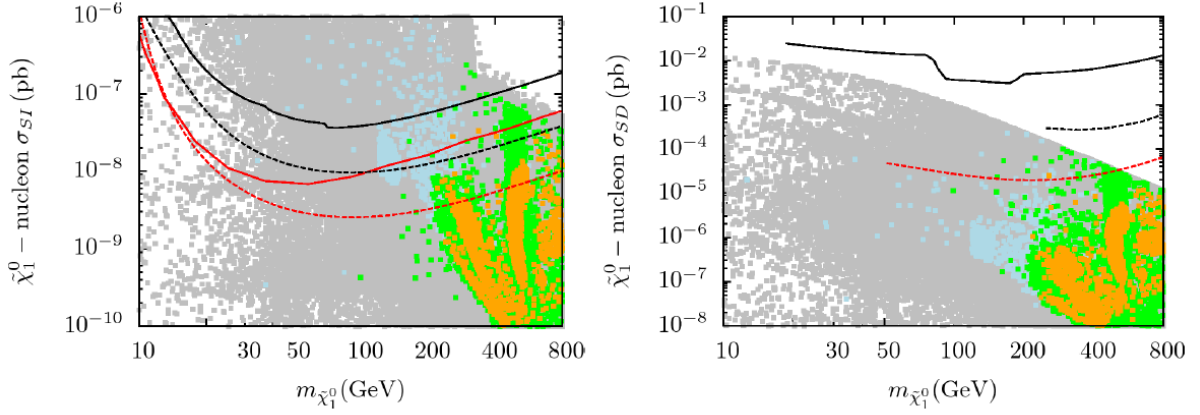


Figure 10: Plots in the $\sigma_{\text{SI}} - m_{\tilde{\chi}_1^0}$ and $\sigma_{\text{SD}} - m_{\tilde{\chi}_1^0}$ planes for Case I. Color coding is the same as in Fig. 1. In the $\sigma_{\text{SI}} - m_{\tilde{\chi}_1^0}$ plane, the current and future bounds are represented by black (solid and dashed) lines for the CDMS experiment and by red (solid and dashed) lines for the Xenon experiment. In the $\sigma_{\text{SD}} - m_{\tilde{\chi}_1^0}$ plane we show the current bounds from Super K (black line) and IceCube (dotted red line) and future reach of IceCube DeepCore (red solid line).

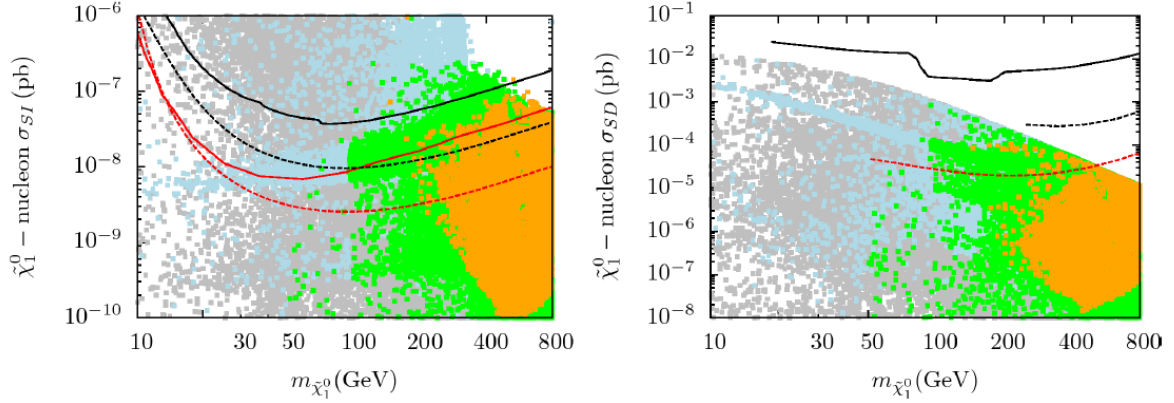


Figure 11: Plots in the $\sigma_{\text{SI}} - m_{\tilde{\chi}_1^0}$ and $\sigma_{\text{SD}} - m_{\tilde{\chi}_1^0}$ planes for Case II. Color coding is the same as in Fig. 1. In the $\sigma_{\text{SI}} - m_{\tilde{\chi}_1^0}$ plane, the current and future bounds are represented by black (solid and dashed) lines for the CDMS experiment and by red (solid and dashed) lines for the Xenon experiment. In the $\sigma_{\text{SD}} - m_{\tilde{\chi}_1^0}$ plane we show the current bounds from Super K (black line) and IceCube (dotted red line) and future reach of IceCube DeepCore (red solid line).

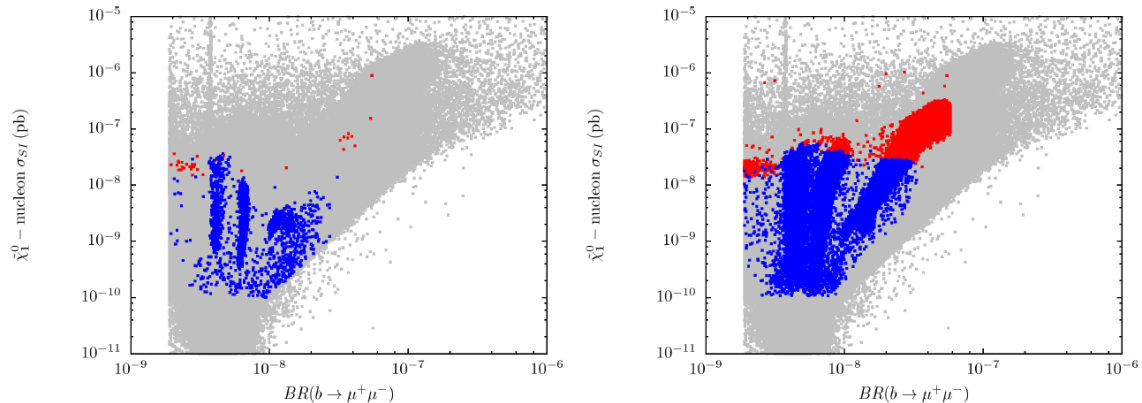


Figure 12: Plots in $\sigma_{SI} - BR(B_s \rightarrow \mu^+ \mu^-)$ for case I (left) and Case II (right) panels in NUHM1 parameter space. Gray points are consistent with REWSB and neutralino LSP. Red points are subset of gray points which are excluded by Xenon100 and CDMS-II experiments. Blue points belong to a subset of gray points consistent with QYU and the experimental constraints discussed in Section 3. Blue points can be tested by Xenon1T experiment [32].

we have examined. The MSSM parameter $\tan \beta$, as expected, turns out to be fairly large in QYU models, of order 54-60. The prospects for testing these ideas in the ongoing experiments is briefly discussed.

Note added: A similar analysis in the CMSSM framework is being carried out by N. Karagiannakis, G. Lazarides and C. Pallis (private communication).

Acknowledgments

We thank Rizwan Khalid, C. Pallis and Shabbar Raza for valuable discussions. This work is supported in part by the DOE Grant No. DE-FG02-91ER40626 (I.G., C.U., and Q.S.) and GNSF Grant No. 07_462_4-270 (I.G.).

References

- [1] B. Ananthanarayan, G. Lazarides and Q. Shafi, Phys. Rev. D **44**, 1613 (1991) and Phys. Lett. B **300**, 24 (1993)5; Q. Shafi and B. Ananthanarayan, Trieste HEP Cosmol.1991:233-244.
- [2] L. J. Hall, R. Rattazzi and U. Sarid, Phys. Rev. D **50**, 7048 (1994); M. Olechowski and S. Pokorski, Phys. Lett. B **214**, 393 (1988); T. Banks, Nucl. Phys.

- B **303**, 172 (1988); V. Barger, M. Berger and P. Ohmann, Phys. Rev. D **49**, (1994) 4908; M. Carena, M. Olechowski, S. Pokorski and C. Wagner, Nucl. Phys. B **426**, 269 (1994); B. Ananthanarayan, Q. Shafi and X. Wang, Phys. Rev. D **50**, 5980 (1994); G. Anderson et al. Phys. Rev. D **47**, (1993) 3702 and Phys. Rev. D **49**, 3660 (1994); R. Rattazzi and U. Sarid, Phys. Rev. D **53**, 1553 (1996); T. Blazek, M. Carena, S. Raby and C. Wagner, Phys. Rev. D **56**, 6919 (1997); T. Blazek, S. Raby and K. Tobe, Phys. Rev. D **62**, 055001 (2000); H. Baer, M. Diaz, J. Ferrandis and X. Tata, Phys. Rev. D **61**, 111701 (2000); H. Baer, M. Brhlik, M. Diaz, J. Ferrandis, P. Mercadante, P. Quintana and X. Tata, Phys. Rev. D **63**, 015007(2001); C. Balazs and R. Dermisek, JHEP **0306**, 024 (2003); C. Pallis, Nucl. Phys. B **678**, 398 (2004); U. Chattopadhyay, A. Corsetti and P. Nath, Phys. Rev. D **66** 035003, (2002); T. Blazek, R. Dermisek and S. Raby, Phys. Rev. Lett. **88**, 111804 (2002) and Phys. Rev. D **65**, 115004 (2002); M. Gomez, T. Ibrahim, P. Nath and S. Skadhauge, Phys. Rev. D **72**, 095008 (2005); K. Tobe and J. D. Wells, Nucl. Phys. B **663**, 123 (2003); I. Gogoladze, Y. Mimura, S. Nandi, Phys. Lett. **B562**, 307 (2003); W. Altmannshofer, D. Guadagnoli, S. Raby and D. M. Straub, Phys. Lett. B **668**, 385 (2008); S. Antusch and M. Spinrath, Phys. Rev. D **78**, 075020 (2008); H. Baer, S. Kraml and S. Sekmen, JHEP **0909**, 005 (2009); S. Antusch and M. Spinrath, Phys. Rev. D **79**, 095004 (2009); D. Guadagnoli, S. Raby and D. M. Straub, JHEP **0910**, 059 (2009); K. Choi, D. Guadagnoli, S. H. Im and C. B. Park, JHEP **1010**, 025 (2010).
- [3] H. Baer, S. Kraml, S. Sekmen and H. Summy, JHEP **0803**, 056 (2008); H. Baer, M. Haider, S. Kraml, S. Sekmen and H. Summy, JCAP **0902**, 002 (2009); I. Gogoladze, R. Khalid and Q. Shafi, Phys. Rev. D **79**, 115004 (2009);
- [4] H. Baer, S. Kraml, A. Lessa and S. Sekmen, JHEP **1002**, 055 (2010); D. Feldman, Z. Liu and P. Nath, Phys. Rev. D **80**, 015007 (2009); M. A. Ajaib, T. Li, Q. Shafi and K. Wang, JHEP **1101**, 028 (2011).
- [5] M. Olechowski and S. Pokorski, Phys. Lett. B **344**, 201 (1995); D. Matalliotakis and H. P. Nilles, Nucl. Phys. B **435**, 115 (1995); H. Murayama, M. Olechowski and S. Pokorski, Phys. Lett. B **371**, 57 (1996).
- [6] A. Chamseddine, R. Arnowitt and P. Nath, Phys. Rev. Lett. **49** (1982) 970; R. Barbieri, S. Ferrara and C. Savoy, Phys. Lett. **B119** (1982) 343; N. Ohta, Prog. Theor. Phys. **70** (1983) 542; L. J. Hall, J. D. Lykken and S. Weinberg, Phys. Rev. **D27** (1983) 2359; for a review see S. Weinberg, *The Quantum Theory of Fields: Volume 3, Supersymmetry*, Cambridge University Press (2000) 442p.
- [7] I. Gogoladze, R. Khalid, S. Raza and Q. Shafi, arXiv:1102.0013 [hep-ph].

- [8] M. Drees, Phys. Lett. B **181**, 279 (1986); C. F. Kolda and S. P. Martin, Phys. Rev. D **53**, 3871 (1996) [arXiv:hep-ph/9503445].
- [9] I. Gogoladze, R. Khalid and Q. Shafi, Phys. Rev. D **80**, 095016 (2009); I. Gogoladze, R. Khalid, S. Raza and Q. Shafi, arXiv:1008.2765 [hep-ph];
- [10] G. Lazarides, Q. Shafi, C. Wetterich, Nucl. Phys. **B181**, 287 (1981).
- [11] M. E. Gomez, G. Lazarides and C. Pallis, Nucl. Phys. B **638**, 165 (2002); M. E. Gomez, G. Lazarides and C. Pallis, Phys. Rev. D **67**, 097701 (2003); C. Pallis and M. E. Gomez, arXiv:hep-ph/0303098.
- [12] E. Komatsu *et al.* [WMAP Collaboration], Astrophys. J. Suppl. **180**, 330 (2009).
- [13] J. C. Pati and A. Salam, Phys. Rev. D **10**, 275 (1974).
- [14] B. Bajc, A. Melfo, G. Senjanovic and F. Vissani, Phys. Rev. D **70**, 035007 (2004); S. Bertolini, M. Frigerio, M. Malinsky, Phys. Rev. **D70**, 095002 (2004); B. Dutta, Y. Mimura, R. N. Mohapatra, Phys. Rev. **D69**, 115014 (2004); T. Fukuyama, A. Ilakovac, T. Kikuchi, S. Meljanac and N. Okada, J. Math. Phys. **46**, 033505 (2005).
- [15] H. Baer, F. E. Paige, S. D. Protopopescu and X. Tata, arXiv:hep-ph/0001086.
- [16] J. Hisano, H. Murayama, and T. Yanagida, Nucl. Phys. **B402** (1993) 46. Y. Yamada, Z. Phys. **C60** (1993) 83; J. L. Chkareuli and I. G. Gogoladze, Phys. Rev. D **58**, 055011 (1998).
- [17] D. M. Pierce, J. A. Bagger, K. T. Matchev, and R.-j. Zhang, Nucl. Phys. **B491** (1997) 3.
- [18] K. Nakamura *et al.* [Particle Data Group Collaboration], J. Phys. G **G37**, 075021 (2010).
- [19] [Tevatron Electroweak Working Group and CDF Collaboration and D0 Collab], arXiv:0903.2503 [hep-ex].
- [20] See for instance J. R. Ellis, S. F. King and J. P. Roberts, JHEP **0804**, 099 (2008); H. Baer, A. Mustafayev, E. K. Park and X. Tata, JHEP **0805**, 058 (2008) and references therein.
- [21] G. Belanger, F. Boudjema, A. Pukhov and R. K. Singh, JHEP **0911**, 026 (2009); H. Baer, S. Kraml, S. Sekmen and H. Summy, JHEP **0803**, 056 (2008).
- [22] H. Baer, C. Balazs, and A. Belyaev, JHEP **03** (2002) 042; H. Baer, C. Balazs, J. Ferrandis, and X. Tata Phys. Rev. **D64** (2001) 035004.

- [23] S. Schael *et al.* Eur. Phys. J. C **47**, 547 (2006).
- [24] T. Aaltonen *et al.* [CDF Collaboration], Phys. Rev. Lett. **100**, 101802 (2008).
- [25] E. Barberio *et al.* [Heavy Flavor Averaging Group], arXiv:0808.1297 [hep-ex].
- [26] Z. Ahmed *et al.* [The CDMS-II Collaboration], Science **327**, 1619 (2010).
- [27] E. Aprile *et al.* [XENON100 Collaboration], arXiv:1104.2549 [astro-ph.CO].
- [28] For a recent discussion see I. Gogoladze, R. Khalid, Y. Mimura and Q. Shafi, arXiv:1012.1613 [hep-ph] and references therein.
- [29] T. Bruch, f. t. C. Collaboration, arXiv:1001.3037 [astro-ph.IM].
- [30] S. Desai *et al.* [Super-Kamiokande Collaboration], Phys. Rev. D **70**, 083523 (2004) [Erratum-ibid. D **70**, 109901 (2004)].
- [31] R. Abbasi *et al.* [ICECUBE Collaboration], Phys. Rev. Lett. **102**, 201302 (2009).
- [32] The XENON Dark Matter Project
http://xenon.astro.columbia.edu/XENON100_Experiment/